

# Bioactivity of Leucite Containing Glass-ceramics Using Natural Raw Materials

Franco Matías Stábile\*, Cristina Volzone

Centro de Tecnología de Recursos Minerales y Cerámica – CETMIC, CONICET CCT La Plata-CICPBA.  
Camino Centenario y 506, M.B. Gonnet, C.P.1897, Provincia de Buenos Aires, Argentina

Received: February 7, 2014; Revised: June 24, 2014

Glass compositions were carefully prepared, using natural quartz and potassium feldspar as a part of the starting raw materials. The solids were prepared so as to have theoretical stoichiometric leucite and 45S5 Bioglass in different L/Bg weight ratios between 0.43-1.00. Novel bioactive glass-ceramics, containing leucite, sodium calcium silicate and silicorhenanite, confirmed by XRD and FTIR, were obtained. Bioactivity tests were carried out on powdered and sintered disks forms. The immersion time was up to 25 days. Apatite formation on powders was studied by FTIR, and XRD and SEM were used to study bioactivity on disks. The materials developed an apatite layer on their surfaces within 6 days of immersion in simulated body fluid. The glass-ceramic with L/Bg ratio= 0.43 presented an apatite layer on all its surface, not so for the samples with 0.66 and 1.00 ratios, on which such layer was peeled off in most part of their surfaces.

**Keywords:** *leucite, glass-ceramics, bioactivity, feldspar, quartz*

## 1. Introduction

Bioglass 45S5 is the best known bioceramic and the most used in clinical applications for its rapid hydroxycarbonate apatite (HCA) layer formation which allows bone tissue bonding. In spite of these advantages, it has some drawbacks such as its low mechanical resistance and its high dissolution rate. A good mechanical resistance and a controlled dissolution rate are necessary key properties in tissue engineering. A way to solve this problem and control degradation rate is heat treating Bioglass so as to turns it into a glass-ceramic. The latter slightly decreases the kinetics of HA formation without suppressing its bioactivity, as it has been demonstrated by many authors<sup>1-4</sup>. Another form to fulfill the mechanical resistant requirements is by carefully designing the composition of the precursor glass so that it develops, together with thermal treatment, crystalline phases which reinforce the material. Aluminum addition is another way to improve mechanical properties and control the degradation rate of glass, but it cannot surpass 3 % w/w, otherwise, it inhibits bone bonding<sup>5</sup>. Nevertheless, if Al ions are part of a crystalline phase, there is no interference with the bioactivity, as is the case of mica-apatite glass-ceramics<sup>6,7</sup>. All of these materials are mostly produced from analytical grade raw materials.

Leucite is widely used in dental glass-ceramics as a reinforcing phase<sup>8</sup>. Studies have been made to evaluate bioactive glass-ceramics composites containing leucite for dental application<sup>9,10</sup>. In this work, it was able to produce glass-ceramics containing sodium calcium silicate and leucite as mayor phases, but not by mixing two glasses that have different composition, as it is the case of glass-ceramics composites. To our knowledge, there is no research not only on bioactive glass-ceramics containing leucite that was not

produced from composites, neither on using natural minerals as starting materials.

The aim of this work was to strategically prepare glasses that develop leucite crystals using natural minerals and analytical grade raw materials as well as to evaluate glass-ceramics bioactivity.

## 2. Experimental

### 2.1. Sample preparation

The raw materials used were analytical grade sodium carbonate, calcium carbonate, monobasic ammonium phosphate (Anedra) and potassium carbonate (Biopack); and high purity natural quartz and potassium feldspar provided by a national mining company. Table 1 shows the chemical analyses of the natural raw materials.

Glass compositions were prepared so as to have theoretical weight ratios of stoichiometric leucite ( $\text{KAlSi}_2\text{O}_6$ ) and 45S5 Bioglass between 0.43-1.00. In this way, three glasses were produced: L30Bg70 (L/Bg=0.43), L40Bg60 (L/Bg=0.66) and L50Bg50 (L/Bg=1.00), where the number next to L is the theoretical weight percentage of Leucite and the number next to Bg is the theoretical weight percentage of Bioglass 45S5. All mixtures were prepared using a ball mill with ethanol during one hour. The mixtures were pre-treated for decarbonation for 4 hours at 900 °C. Glass frits were produced by melting at 1550 °C for one hour and quenched into distilled water. Frits were milled into porcelain mortar and passed through 200 mesh. Glass-ceramics powder were produced by heat-treating loose glass powders onto platinum plates, grounded into porcelain mortar and then sieved through 100 mesh. Glass-ceramics disks were

\*e-mail: [mstabile@cetmic.unlp.edu.ar](mailto:mstabile@cetmic.unlp.edu.ar)

produced by heat treatment of glass powders pressed up to 140 MPa in cylindrical shape. These heat treatments were the same for powders and disks and were performed at a heating rate of 2 °C per minute up to each glass softening temperature, which were obtained by thermal analyses (920, 990 and 1000 °C for L30Bg70, L40Bg60 and L50Bg50, respectively), holding the temperature for 2 hours.

## 2.2. Bioactivity test

Glass-ceramics in powders and disks forms were assessed in simulated body fluid (SBF) for 6 and 25 days. The solid/solution ratios were 1mg/cm<sup>3</sup> for powders and 0.1cm<sup>-1</sup> for disks. The solution was renewed every 5 days. Simulated body fluid was prepared following the recipe given by Kokubo et al.<sup>11</sup>.

## 2.3. XRD

Glass-ceramic disks before and after assessment in simulated body fluid and powder glass-ceramics after thermal treatments were characterized by X-ray diffraction on a Philips 3010 equipment using Cu K $\alpha$  radiation ( $\lambda = 1.5405 \text{ \AA}$ ) at 40kV and 35 mA. Powdered glass-ceramics diffractograms were obtained using a step of 0.04 °(2 $\theta$ ) and 2 seconds per step, from 10 to 70 °(2 $\theta$ ), for crystalline phase determination. Diffractograms of the surfaces of glass-ceramics disks were obtained using a step of 0.03 °(2 $\theta$ ) and 4 seconds per step, from 22.49 to 35.00 °(2 $\theta$ ), to get more sensibility for apatite detection.

## 2.4. FTIR

Fourier transformed infrared spectra (4000-380 cm<sup>-1</sup>) of powdered glass-ceramics before and after SBF immersion were measured by using Spectrum One Perkin Elmer equipment in transmittance mode. The samples were dispersed in KBr (1% mass) and compacted in a thin pellet form.

## 2.5. SEM

The surfaces of reacted and unreacted glass-ceramics disks were observed using a scanning electron microscope FEI Quanta 200, at 20 kV and low vacuum. The Ca/P ratios of the formed layers were analyzed by EDAX. Samples did not have additional coating for the analyses.

## 3. Results

### 3.1. X-Ray diffraction

X-ray diffraction of L30Bg70, L40Bg60 and L50Bg50 glass-ceramics powders are shown in Figure 1. All samples crystallized after the corresponding thermal treatment. It was found that peaks positions and intensities match with Na<sub>2</sub>CaSi<sub>2</sub>O<sub>6</sub> pattern (sodium calcium silicate), KAlSi<sub>2</sub>O<sub>6</sub> (leucite) and Na<sub>2</sub>Ca<sub>4</sub>(PO<sub>4</sub>)<sub>2</sub>SiO<sub>4</sub> (silicorhenanite) phases.

Both Na<sub>2</sub>CaSi<sub>2</sub>O<sub>6</sub> and Na<sub>2</sub>Ca<sub>4</sub>(PO<sub>4</sub>)<sub>2</sub>SiO<sub>4</sub> were found after thermal treatment of Bioglass 45S5<sup>12,13</sup>. As it can be observed, the relative intensities of the major phases, Na<sub>2</sub>CaSi<sub>2</sub>O<sub>6</sub> and KAlSi<sub>2</sub>O<sub>6</sub>, were different in each sample. The relative peaks intensities of sodium calcium silicate increased, while leucite intensities decreased with the theoretical quantity of Bioglass in composition.

XRD of the surfaces of L30Bg70, L40Bg60 and L50Bg50 glass-ceramics disks before and after assessment in SBF are shown in Figure 2. In these cases, silicorhenanite peaks could not be detected. All glass-ceramics showed a decrease on sodium calcium silicate peaks intensities vs

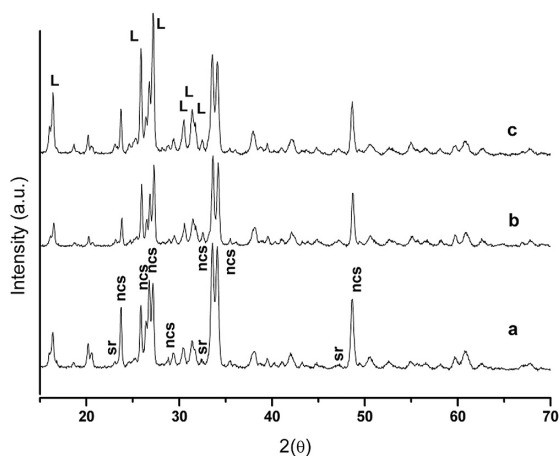


**Figure 1.** XRD of glass-ceramics in powder form: a: L30Bg70; b: L40Bg60; c: L50Bg50. L: leucite; ncs: sodium calcium silicate; sr: silicorhenanite.

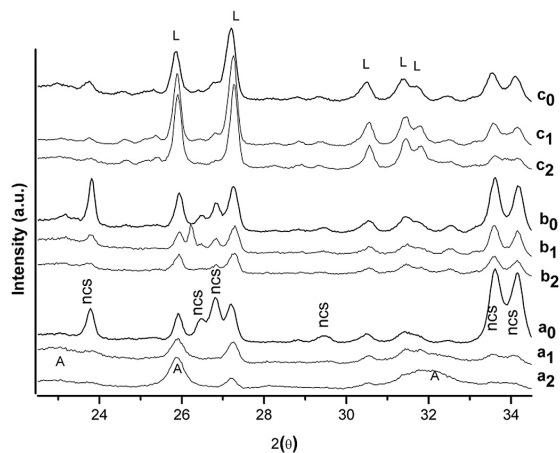


**Figure 2.** XRD of disk glass-ceramics: before (a<sub>0</sub>: L30Bg70; b<sub>0</sub>: L40Bg60; c<sub>0</sub>: L50Bg50) and after 6 (a<sub>1</sub>: L30Bg70; b<sub>1</sub>: L40Bg60; c<sub>1</sub>: L50Bg50) and 25 (a<sub>2</sub>: L30Bg70; b<sub>2</sub>: L40Bg60; c<sub>2</sub>: L50Bg50) days of immersion in SBF solutions. L: leucite; ncs: sodium calcium silicate; A: apatite.

**Table 1.** Chemical analyses of natural raw materials.

Raw Material	SiO <sub>2</sub>	Al <sub>2</sub> O <sub>3</sub>	Na <sub>2</sub> O	K <sub>2</sub> O	CaO	Fe <sub>2</sub> O <sub>3</sub>	TiO <sub>2</sub>
Feldspar	66.25	18.42	2.06	12.02	0.20	0.05	0.01
Quartz	99.33	0.49	0.06	0.10	0.00	0.01	0.00

assessed time in SBF. After the 6<sup>th</sup> day, the diffracted peaks of sodium calcium silicate in L30Bg70 almost disappeared, while for L40Bg60 and L50Bg50, the peaks of this phase were diminished but remained well-visible. The intensities of leucite peaks were slightly diminished on L30Bg70 and L40Bg60 samples, while there was not a noticeable change in L50Bg50.

After the 25<sup>th</sup> day of assessment, the diffraction peaks of sodium calcium silicate were no more detectable in glass-ceramic L30Bg70, while the intensities decreased a little more in L40Bg60 and L50Bg50, but still were distinguishable. Leucite peaks in L30Bg70 were more reduced, except for that at around 26° (2θ) which increased and corresponds to the (0 0 2) plane of hydroxyapatite, and a broad halo appeared at around 32° which is the result of the contribution of the (2 2 1), (1 1 2), and (2 0 2) planes of apatite<sup>14</sup>. This affirmed the establishment of a well-formed hydroxyapatite layer on the surface of L30Bg70 specimen. In contrast, L40Bg60 showed a little more reduction in all leucite intensities and no difference was observed on L50Bg50 with timeless immersions in SBF. Apatite formation was not possible to perceive by X-ray diffraction on L40Bg60 and L50Bg50.

### 3.2. FTIR

Figure 3 shows the Fourier transformed infrared spectra of L30Bg70, L40Bg60 and L50Bg50 glass-ceramics before and after assessment in simulated body fluid.

The unreacted L30Bg70 glass-ceramic showed bands at 1100-1000 cm<sup>-1</sup>, 950-900 cm<sup>-1</sup> and 443 cm<sup>-1</sup> attributed to Si-O-Si, Si-O (NBO)<sup>1,15</sup> stretching, and Si-O-Si bending vibrations<sup>1</sup>, respectively, as well as a band at 619 cm<sup>-1</sup>, all associated with sodium calcium silicate phase<sup>16</sup>. The presence of leucite was evident by the appearance of the band located at 720 cm<sup>-1</sup><sup>17</sup>, and a broadband at 500-560 cm<sup>-1</sup> which coincides also with the contribution of PO bending vibrations of silicorhenanite<sup>18</sup>. The band at 577 cm<sup>-1</sup> corresponds to a crystalline PO bending vibrational mode, which can be also attributed to silicorhenanite<sup>18,19</sup>.

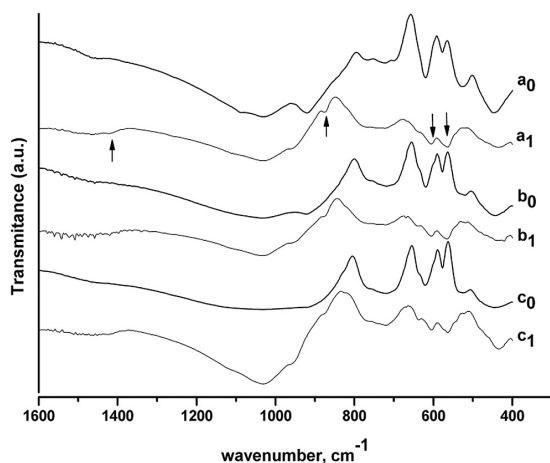


**Figure 3.** Infrared spectra of glass-ceramics before ( $a_0$ : L30Bg70;  $b_0$ : L40Bg60;  $c_0$ : L50Bg50) and after 6 ( $a_1$ : L30Bg70;  $b_1$ : L40Bg60;  $c_1$ : L50Bg50) days of immersion in SBF solutions.

Glass-ceramic L40Bg60 showed similar bands to those described for L30Bg70, apart from two shoulders at 412 and 642 cm<sup>-1</sup><sup>17</sup>, which were attributed to the presence of leucite. A similar behavior was observed in the L50Bg50 glass-ceramic, in which the band at 720 cm<sup>-1</sup> was intensified and the shoulder at 642 cm<sup>-1</sup> was even more marked, which corresponds to a higher relative content of leucite.

After dipping the L30Bg70 glass-ceramic powder for 6 days in SBF, it was observed that the bands corresponding to sodium calcium silicate (1090, 920, 619 and 443 cm<sup>-1</sup>) and silicorhenanite (577 cm<sup>-1</sup>) were not visible. At the same time, two shoulders could be seen at 542 and 642 cm<sup>-1</sup>, corresponding to vibrational bands of leucite<sup>17</sup>, which were previously overlapped with the bands of sodium calcium silicate. New bands appeared at 562 and 602 cm<sup>-1</sup> corresponding to PO bendings vibrations<sup>20</sup>, two shoulders at 960 cm<sup>-1</sup><sup>21</sup> and 1120 cm<sup>-1</sup><sup>22</sup> related to PO vibrational modes, and an intense band at 1030 cm<sup>-1</sup>, related to different vibrational modes of PO<sub>4</sub><sup>-3/9</sup>, all attributed to the formation of crystalline hydroxyapatite<sup>5</sup>. Two bands were observed at 876 and 1422 cm<sup>-1</sup> corresponding to carbonate substitutions into hydroxyapatite<sup>9</sup>.

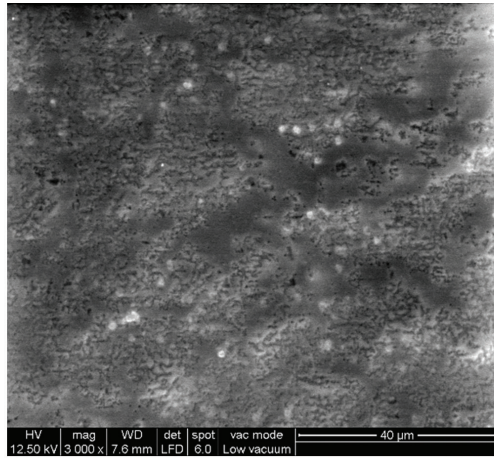
L40Bg60 and L50Bg50 glass-ceramics contacted with SBF for 6 days displayed similar behavior to that described for L30Bg70, with some particularities. In the IR spectrum of reacted L40Bg60, we could see that the bands at 542 and 642 cm<sup>-1</sup>, corresponding to leucite, were more visible and those related to carbonate substitutions into hydroxyapatite decreased in intensity with respect to the behavior of the sample L30Bg70 for the same contact time. These particular differences were intensified in L50Bg50 sample contacted with SBF.

### 3.3. SEM

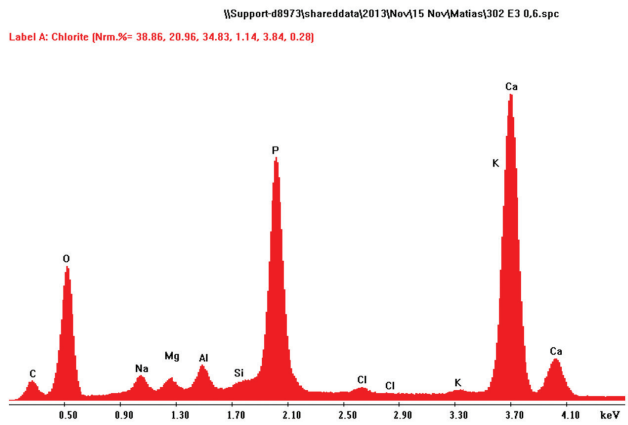
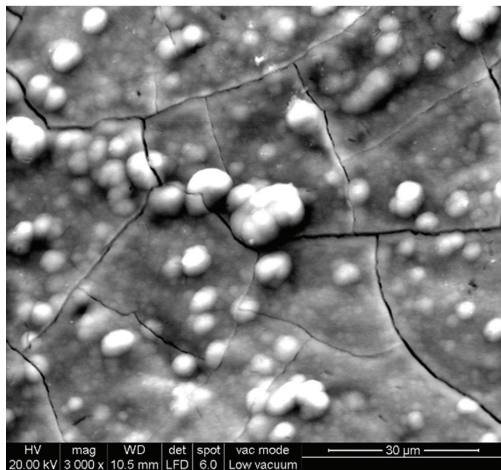
Scanning electron microscope images of the surfaces of glass-ceramics disks before and after assessment in simulated body fluid at different times are displayed in Figures 4, 5 and 6. The three glass-ceramics surfaces before SBF contact have homogeneous characteristics. L30Bg70 glass ceramics presented a rather smooth surface, with a poor rugosity, where glass precursor particles were almost undistinguishable. L40Bg60 and L50Bg50 glass-ceramics showed a more roughened surface than L30Bg70 glass ceramic, with more defined particles with round shapes. After 6 days of immersion, L30Bg70 specimen presented spherical particles of hydroxyapatite that agglomerated and formed a thin smooth layer, with some particles standing out. Chen et. al. found that 45S5 Bioglass-derived glass-ceramics scaffolds formed a HCA layer after 7 days of immersion in SFB<sup>22</sup>. The layer copied the microstructure of the specimen surface and presented cracks, which usually appear because of the shrinking of silica-rich layer when dried, onto which the apatite layer grows. For L40Bg60 and L50Bg50, apatite layer was formed too, but it was only possible to find it close to the edge of the disks, because there was not well adherence to the surface and it had peeled off. The layer had many cracks and it was characterized by a rough morphology of spherical agglomerated apatite particles in both samples. On the 25<sup>th</sup> day, L30Bg70 had a visibly thicker apatite layer and was even smoother so the morphology of the sample surface was no

more noticeable. The layer of L40Bg60 and L50Bg50 glass-ceramics after 25 days of immersion had a lot of outbound apatite particles and the layer was very rough. Again, the layer was only found in some places for both specimens. In

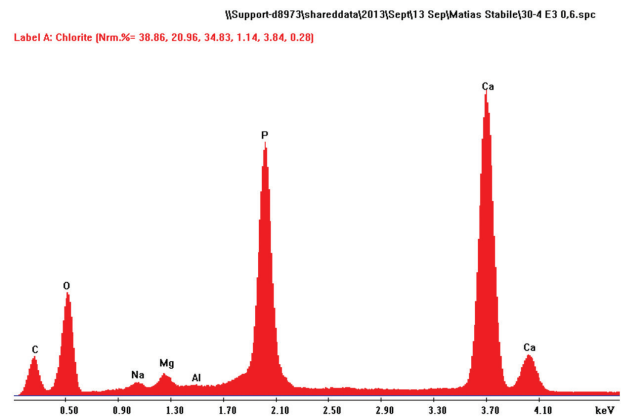
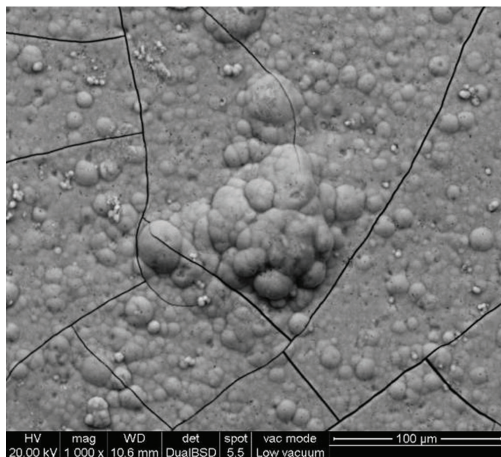
all cases, Ca/P ratios of hydroxyapatite particles and layer were in the range of 1.39-1.58 which indicated the presence of Ca-deficient apatite. This was an important fact since the Ca/P ratio of bone tissue is below 1.67<sup>23,24</sup>.



a<sub>0</sub>



a<sub>1</sub>



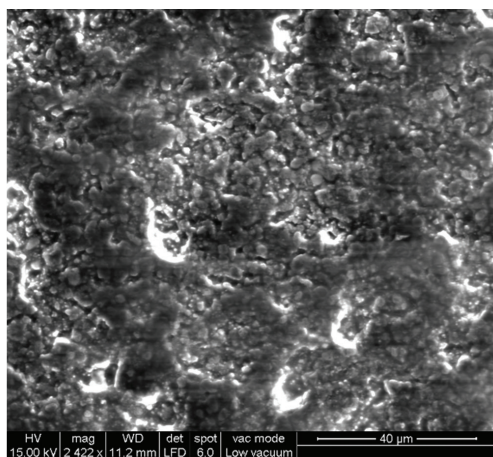
a<sub>2</sub>

**Figure 4.** SEM and EDAX of L30Bg70 glass ceramic before (a<sub>0</sub>) and after 6 (a<sub>1</sub>) and 25 (a<sub>2</sub>) days of immersion in SBF.

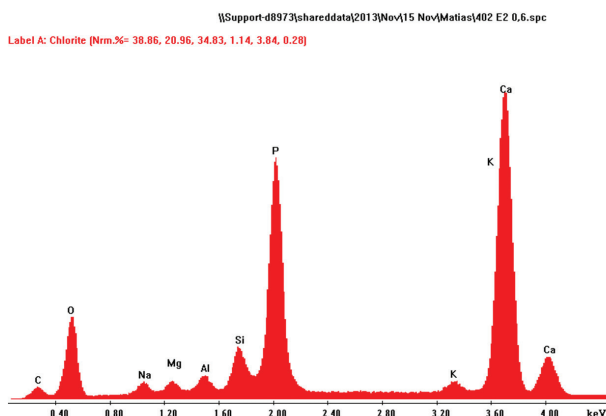
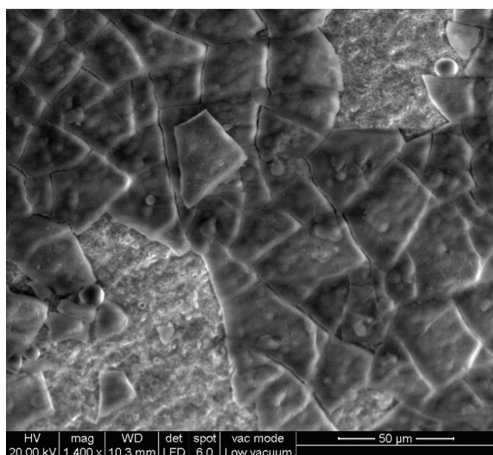
### 4. Discussion

Thermal treatments applied to each glass caused the formation of sintered glass-ceramics. In all cases, the crystallized phases were  $\text{Na}_2\text{CaSi}_2\text{O}_6$ ,  $\text{Na}_2\text{Ca}_4(\text{PO}_4)_2\text{SiO}_4$ ,

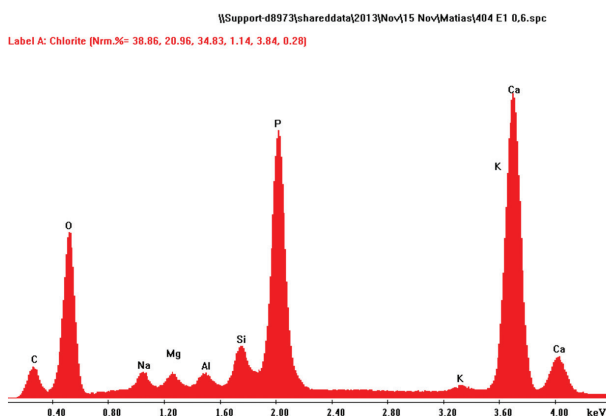
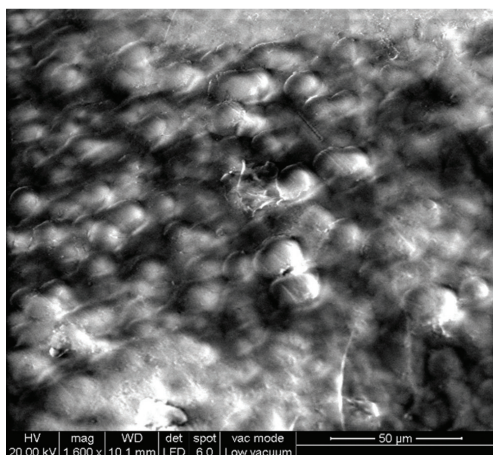
both developed after thermal treatment of Bioglass<sup>12,13</sup> and  $\text{KAlSi}_2\text{O}_6$ . Leucite formation was possible by treating the glass in powder form, which activated the surface crystallization mechanism of the aluminosilicate phase<sup>25</sup>. Sodium calcium silicate was formed by surface



b<sub>0</sub>



b<sub>1</sub>

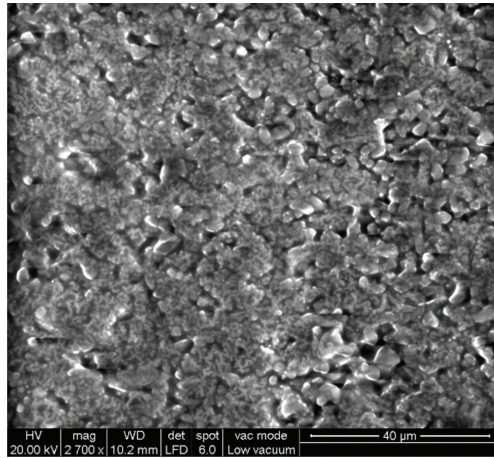


b<sub>2</sub>

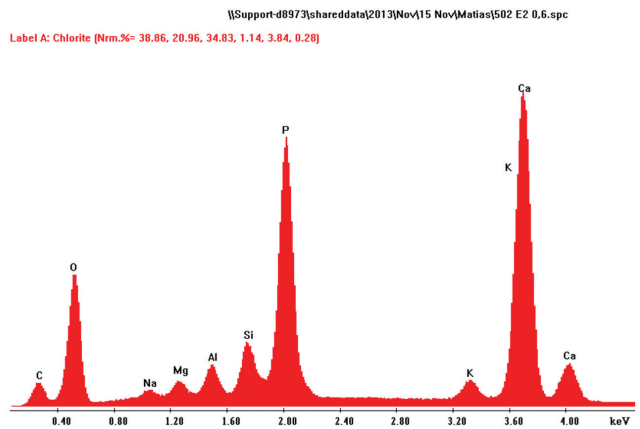
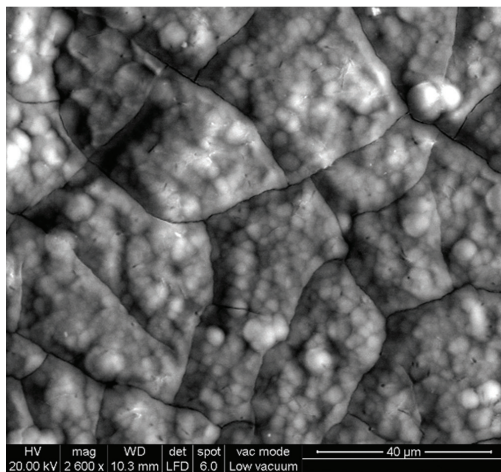
Figure 5. SEM and EDAX of L40Bg60 glass ceramic before (b<sub>0</sub>) and after 6 (b<sub>1</sub>) and 25 (b<sub>2</sub>) days of immersion in SBF.

but not by volume mechanism. The small particle size of precursor glasses promoted surface over volume crystallization<sup>26</sup>. Detection of the silicate phase by XRD on the surfaces of all samples, which was not hindered

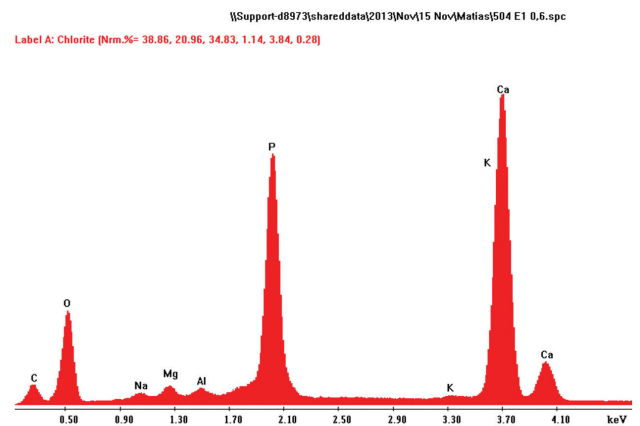
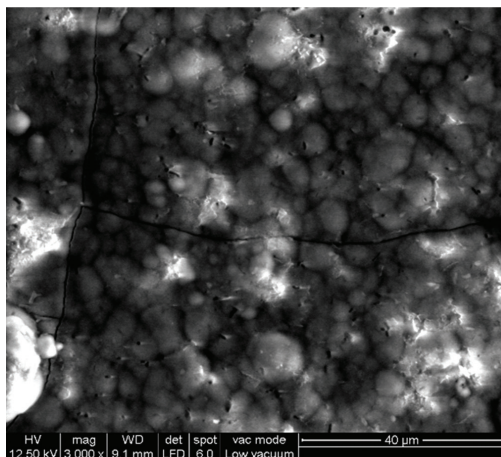
by the surface crystallization of leucite, demonstrated this fact. Nevertheless, silicorhenanite was indeed obstructed by surface crystallization, as its diffraction peaks were not detectable in glass-ceramics disks. As it was expected,



C0



C1



C2

**Figure 6.** SEM and EDAX of L50Bg50 glass ceramic before (c<sub>0</sub>) and after 6 (c<sub>1</sub>) and 25 (c<sub>2</sub>) days of immersion in SBF.

amounts of leucite and sodium calcium silicate decreased and increased respectively with the quantity of Bioglass in the mix.

All samples demonstrated bioactive behavior after 6 days of contact with simulated body fluid in both powdered and sintered disk forms. A well former apatite layer was crystallized in all glass-ceramics in powder form, as it was shown by FTIR. Apatite layer was possible to be detected by SEM at the 6th day in all sintered samples. This layer in L30Bg70 was not thick enough to be detected by X-ray diffraction. A well-formed and thick enough layer was crystallized on the surface of L30Bg70 glass-ceramic after 25 days of immersion, as it was found by X-ray diffraction. L30Bg70 had the highest amount of sodium calcium silicate, which was dissolved in contact with SBF and contributed to the HCA formation<sup>13</sup>, and the lowest amount of non-bioactive leucite of all samples, which could explain its good bioactive behavior. The apatite layer in L40Bg60 and L50Bg50 was not present in all surface after 6 and 25 days of immersion, because it had peeled off, due to the quantity of non-bioactive leucite<sup>27</sup> and it was only found in some places. That is why the HCA layer was not detected by XRD

because it was absent in most of the surface. Nevertheless, this layer was present close to the edge of the disks.

## 5. Conclusions

Bioactive glass-ceramics containing leucite, sodium calcium silicate and silicorhenanite could be obtained using natural raw materials such as quartz and potassium feldspar as part of starting components. The apatite layer on the L30Bg70 (L/Bg=0.43) glass-ceramic disk was well-formed and it was the most bioactive sample. However, the apatite layer was not well-adhered to the surface of the disks because of the higher quantity of leucite in L40Bg60 (L/Bg=0.66) and L50Bg50 (L/Bg=1.00) glass-ceramics. Further studies have to be done to evaluate the possible applications of these new types of bioactive materials.

## Acknowledgements

The authors would like to thank CONICET for its financial support (PIP 0115) and José Ortega for his important technical assistance.

## References

- Peitl O, Zanotto ED and Hench LL. Highly bioactive P2O<sub>5</sub>-Na<sub>2</sub>O-CaO-SiO<sub>2</sub> glass-ceramics. *Journal of Non-Crystalline Solids*. 2001; 292(1-3):115-126. [http://dx.doi.org/10.1016/S0022-3093\(01\)00822-5](http://dx.doi.org/10.1016/S0022-3093(01)00822-5)
- Peitl O, La Torre G and Hench LL. Effect of crystallization on apatite layer formation of bioactive glass 45S5. *Journal of Biomedical Materials Research*. 1996; 30(4):509-514. [http://dx.doi.org/10.1002/\(SICI\)1097-4636\(199604\)30:4<509::AID-JBM9>3.0.CO;2-T](http://dx.doi.org/10.1002/(SICI)1097-4636(199604)30:4<509::AID-JBM9>3.0.CO;2-T)
- Moura J, Teixeira LN, Ravagnani C, Peitl O, Zanotto ED and Beloti MM. In Vitro osteogenesis on a highly bioactive glass-ceramic (Biosilicate). *Journal of Biomedical Materials Research Part A*. 2007; 82A(3):545-557. PMID:17311315. <http://dx.doi.org/10.1002/jbm.a.31165>
- Jabur OR and Barros VMR. Bone formation on Ti implants in intra-bony defects sites filled with different bone substitutes: histomorphometric analysis in dogs. In: *International Congress of Implantology*; 2008; Ribeirão Preto, Brazil.
- Hench LL. Bioceramics: from concept to clinic. *Journal of the American Ceramic Society*. 1991; 74(7):1487-1510. <http://dx.doi.org/10.1111/j.1151-2916.1991.tb07132.x>
- Liu Y, Sheng X, Dan X and Xiang Q. Preparation of mica/apatite glass-ceramics biomaterials. *Materials Science and Engineering: C*. 2006; 26(8):1390-1394. <http://dx.doi.org/10.1016/j.msec.2005.08.017>
- Xiang Q, Liu Y, Sheng X and Dan X. Preparation of mica based glass-ceramics with needle-like fluorapatite. *Dental Materials*. 2007; 23(2):251-258. PMID:17134748. <http://dx.doi.org/10.1016/j.dental.2006.10.008>
- Cattella MJ, Chadwick TC, Knowles JC and Clarke RL. The crystallization of an aluminosilicate glass in the K<sub>2</sub>O-Al<sub>2</sub>O<sub>3</sub>-SiO<sub>2</sub> system. *Dental Materials*. 2005; 21(9):811-822. PMID:15961153. <http://dx.doi.org/10.1016/j.dental.2005.02.001>
- Manda M, Goudouri OM, Papadopoulou L, Kantiranis N, Christofilos D, Triantafyllidis K et al. Material characterization and bioactivity evaluation of dental porcelain modified by bioactive glass. *Ceramics International*. 2012; 38(7):5585-5596. <http://dx.doi.org/10.1016/j.ceramint.2012.03.078>
- Kontonasaki E, Papadopoulou L, Zorba T, Pavlidou E, Paraskevopoulos K and Koidis P. Apatite formation on dental ceramics modified by a bioactive glass. *Journal of Oral Rehabilitation*. 2003; 30(9):893-902. PMID:12950970. <http://dx.doi.org/10.1046/j.1365-2842.2003.01072.x>
- Kokubo T, Kushitani H, Sakka S, Kitsugi T and Yamamuro T. Solutions able to reproduce in vivo surface-structure changes in bioactive glass-ceramic A-W. *Journal of Biomedical Materials Research*. 1990; 24(6):721-734. PMID:2361964. <http://dx.doi.org/10.1002/jbm.820240607>
- Lefebvre L, Chevalier J, Gremillard L, Zenati R, Thollet G, Bernache-Assollant D et al. Structural transformations of bioactive glass 45S5 with thermal treatments. *Acta Materialia*. 2007; 55(10):3305-3313. <http://dx.doi.org/10.1016/j.actamat.2007.01.029>
- Magallanes-Perdomo M, Meille S, Chenal JM, Pacard E and Chevalier J. Bioactivity modulation of Bioglass® powder by thermal treatment. *Journal of the European Ceramic Society*. 2012; 32(11):2765-2775. <http://dx.doi.org/10.1016/j.jeurceramsoc.2012.03.018>
- Chou YF, Chiou WA, Xu Y, Dunn JC and Wu BM. The effect of pH on the structural evolution of accelerated biomimetic apatite. *Biomaterials*. 2004; 25(22):5323-5331. PMID:15110483. <http://dx.doi.org/10.1016/j.biomaterials.2003.12.037>
- Gomez-Vega JM, Saiz E, Tomsia AP, Marshall GW and Marshall SJ. Bioactive glass coatings with hydroxyapatite and Bioglass particles on Ti-based implants. *Biomaterials*. 2000; 21(2):105-111. [http://dx.doi.org/10.1016/S0142-9612\(99\)00131-3](http://dx.doi.org/10.1016/S0142-9612(99)00131-3)
- Bretcanu O, Chatzistavrou X, Paraskevopoulos K, Conrad R, Thompson I and Boccaccini AR. Sintering and crystallisation of 45S5 Bioglass® powder. *Journal of the European Ceramic Society*. 2009; 29(16):3299-3306. <http://dx.doi.org/10.1016/j.jeurceramsoc.2009.06.035>
- Music S, Zivko-Babic J, Mehulic K, Ristic M, Popovic S and Furic K. Microstructure of leucite glass-ceramics for dental

- use. *Materials Letters*. 1996; 27(4-5):195-199. [http://dx.doi.org/10.1016/0167-577X\(95\)00280-4](http://dx.doi.org/10.1016/0167-577X(95)00280-4)
18. Chatzistavrou X, Zorba T, Kontonasaki E, Chryssafis K, Koidis P and Paraskevopoulos K. Following bioactive glass behavior beyond melting point by thermal and optical methods. *Physica Status Solidi (a)*. 2004; 201(5):944-951. <http://dx.doi.org/10.1002/pssa.200306776>
  19. Smith BC. *Infrared spectral interpretation: a systematic approach*. Boca Raton: CRC Press; 1999.
  20. Goudouri OM, Kontonasaki E, Theocharidou A, Papadopoulou L, Kantiranis N, Chatzistavrou X et al. Modifying a dental ceramic by bioactive glass via the sol-gel route: characterization and bioactivity investigation. *Materials Chemistry and Physics*. 2011; 125(1-2):309-313. <http://dx.doi.org/10.1016/j.matchemphys.2010.09.054>
  21. Vaid C and Murugavel S. Alkali oxide containing mesoporous bioactive glasses: Synthesis, characterization and in vitro bioactivity. *Materials Science and Engineering: C*. 2013; 33(2):959-968. <http://dx.doi.org/10.1016/j.msec.2012.11.028>
  22. Chen QZ, Thompson ID and Boccaccini AR. 45S5 Bioglass®-derived glass-ceramic scaffolds for bone tissue engineering. *Biomaterials*. 2006; 27(11):2414-2425. PMID:16336997. <http://dx.doi.org/10.1016/j.biomaterials.2005.11.025>
  23. Deng XM, Hao JY and Wang CS. Preparation and mechanical properties of nanocomposites of poly(D,L-lactide) with Ca-deficient hydroxyapatite nanocrystals. *Biomaterials*. 2001; 22(21):2867-2873. [http://dx.doi.org/10.1016/S0142-9612\(01\)00031-X](http://dx.doi.org/10.1016/S0142-9612(01)00031-X)
  24. Li YB, De Wijn J, Klein CPAT and Van de Meer S. Preparation and characterization of nanograde osteoapatite-like rod crystals. *Journal of Materials Science: Materials in Medicine*. 1994; 5(5):252-255. <http://dx.doi.org/10.1007/BF00122393>
  25. Höland W, Frank M and Rheinberger V. Realstruktur und Gefüge der Empress Glaskeramik nach Aetzung. *Quintessenz*. 1993; 44:761-773 .
  26. Chatzistavrou X, Zorba T, Chrissafis K, Kaimakamis G, Kontonasaki E, Koidis P et al. Influence of particle size on the crystallization process and the bioactive behavior of a bioactive glass system. *Journal of Thermal Analysis and Calorimetry*. 2006; 85(2):253-260. <http://dx.doi.org/10.1007/s10973-005-7165-y>
  27. Verne E, Brovaron CV and Moisescu C. Glazing of alumina by fluoroapatite-containing glass-ceramic. *Journal of Materials Science*. 2005; 40(5):1209-1215. <http://dx.doi.org/10.1007/s10853-005-6939-8>